International Journal of Modern Physics A
Vol. 35, No. 22 (2020) 2050127 (12 pages)

DOI: 10.1142/S0217751X20501274

Investigating the impact of the partonic structure on the description of hadronic collisions at high energies

M. Broilo,* V. P. Gonçalves† and P. V. R. G. Silva‡

High and Medium Energy Group,
Instituto de Física e Matemática, Universidade Federal de Pelotas,
Caixa Postal 354, CEP 96010-900, Pelotas, RS, Brazil
**mateus.broilo@ufrgs.br*
†*barros@ufpel.edu.br*
‡*pvrgsilva@ufpel.edu.br*

Received 27 May 2020
Revised 3 July 2020
Accepted 6 July 2020
Published 7 August 2020

The impact of the partonic structure on the description of the hadronic cross-sections is investigated considering a multichannel eikonal model based on the Good–Walker approach. The total, elastic and single diffractive cross-sections are estimated considering different parametrizations for the parton distribution functions and the predictions are compared with the experimental data for proton–proton (pp) and antiproton–proton ($\bar{p}p$) collisions. We show that the description of the high-energy behavior of the hadronic cross-sections is sensitive to the partonic structure.

Keywords: Quantum chromodynamics; hadron–hadron collisions; single diffraction; partonic structure.

PACS numbers: 13.85.Dz, 13.85.Lg

1. Introduction

During the last year, the TOTEM experiment at the LHC has released precise measurements of proton–proton elastic, inelastic and total cross-sections as well as measurements of the ratio of the real-to-imaginary part of the forward elastic scattering amplitude, *a.k.a.* ρ-parameter.[1–4] Up to now these measurements represent the highest center-of-mass (CM) energy ever achieved in a collider. Over the last few years an intense debate has enhanced the interest in the subject and become a key source of information for selecting phenomenological models and

†Corresponding author.

theoretical approaches to understand, in a deeper level, the theory of strong interactions. Presently, it is widely known that total, elastic, diffractive and inelastic cross-sections rise with increasing energy[5,6] and also that they are dominated by partonic processes with low transferred momenta. The treatment of these reactions in a reliable way within Quantum Chromodynamics (QCD) constitutes one of the main challenges of the theory of the strong interactions.

Over the last decades, many phenomenological models based on Regge–Gribov theory or inspired on QCD were proposed,[7–35] which were able, in most cases, to give a fine description of the pre-LHC[36] and post-LHC[1–4,37–42] experimental results. In particular, in Ref. 35 we have proposed a phenomenological model for the description of the total, elastic cross-sections as well as the treatment of single and double diffractive excitation in pp collisions at high energies. Such model is based on the Good–Walker approach,[43] with the cross-sections being expressed in terms of the eigenstates of the scattering operator and the scattering amplitude of the interaction between them. The results presented in Ref. 35 demonstrated that the model is able to describe the current data for the energy dependence of the cross-sections. Another important aspect shown in Ref. 35 is that the high-energy behavior of the cross-sections is driven by perturbative QCD. As a consequence, the predictions are dependent on the description of the partonic structure of the incident hadrons. Previously, we have assumed that this structure is described by the post-LHC fine-tuned leading-order parametrization proposed by the CTEQ-TEA group in Ref. 44, denoted CT14 hereafter. Our goal in this paper is to complement the study performed in Ref. 35 by investigating the impact of different parametrizations for the parton distributions functions on the description of the hadronic cross-sections. In our analysis, we will compare the CT14 predictions with those derived using the NNPDF31[45] and MMHT[46] parametrizations, both at leading order. Differently from the CT14 parametrization, which only provides the best-fit result for the leading order PDFs, the NNPDF and MMHT groups have estimated the uncertainty on the leading order PDFs due to the errors on the data included in the fit and provided the central value and the one-sigma PDF uncertainty bands. Such uncertainties will be taken into account in the predictions for the total, elastic and diffractive cross-sections. As shown in Fig. 1, these three parametrizations predict very distinct behaviors for the distribution of u-quarks (left panel) and gluons (right panel) at small values of the Bjorken-x variable. In particular, the predictions for very small-x are dependent on the model assumed to extrapolated the PDFs beyond the current kinematical range probed by the data. Such differences are expected to modify the asymptotic behavior of the hadronic cross-sections. As in Ref. 35, we will constrain the main parameters of the model using the recent LHC data for the total cross-section. It will allow us to derive parameter free predictions for the elastic and total single diffractive cross-sections, which will be compared with the current data. As we will show below, our results indicate that the description of the current experimental data at high energies is sensitive to the modeling of the partonic structure.

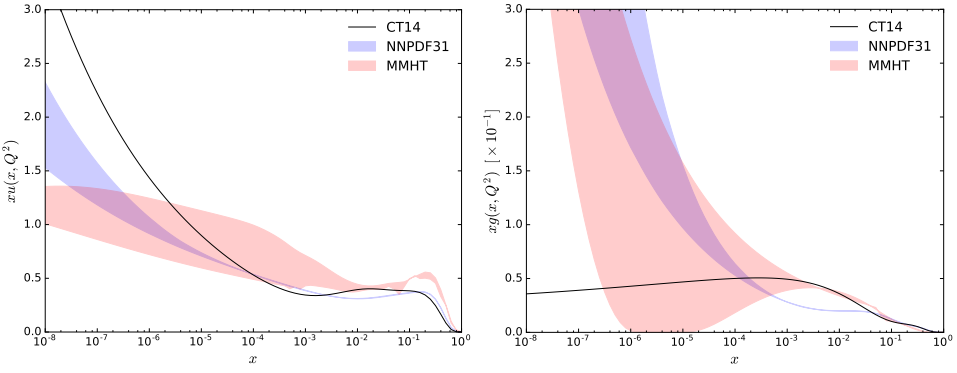

Fig. 1. Bjorken-x dependence of the u-quark (left panel) and gluon (right panel) distributions for $Q^2 = 1.69$ GeV^2 predicted by CT14, NNPDF31 and MMHT parametrizations. The bands for MMHT and NNPDF31 were estimated from the PDFs uncertainties.

The paper is organized as follows. In Sec. 2, we present a brief review of the model proposed in Ref. 35. The derivation of the total, elastic and single diffractive cross-sections in the Good–Walker approach is reviewed and the models for the description of the eigenstates and scattering amplitude are presented. In Sec. 3 the main parameters of the model are determined using the recent LHC data for the total cross-section. Predictions for the elastic and total single diffractive cross-sections are obtained considering distinct parametrizations for the parton distribution functions and the results are compared with the current data. Finally, in Sec. 4, our main conclusions are summarized.

2. Formalism

In order to present the basic aspects from the Good–Walker approach,[43] let us consider the collision between a projectile P and a target T, which can be represented by the physical states $|P\rangle$ and $|T\rangle$, respectively. For simplicity, we will assume that only the projectile state has a substructure and can be diffracted into various particle states $\{|A\rangle\}$. In the Good–Walker approach,[43] the physical state of the incoming hadron $|P\rangle$ is written in terms of the eigenstates of the scattering operator $\hat{T}$, $\{|\psi_k\rangle\}$, with $\mathrm{Im}\,\hat{T}|\psi_k\rangle = t_k|\psi_k\rangle$. Since the eigenstates form a complete set of orthogonal states we can write $|P\rangle = \sum_k C_k|\psi_k\rangle$. So that for the elastic scattering we have

$$\langle P|\hat{T}|P\rangle = \sum_k |C_k|^2 t_k = \langle t\rangle\,. \tag{1}$$

Therefore, the elastic differential cross-section is given by

$$\frac{d^2\sigma_{\rm el}}{d^2b} = \langle t\rangle^2\,, \tag{2}$$

where b is the impact parameter of the collision and we have assumed that the eigenstates are purely imaginary. Using the optical theorem, the total cross-section

distribution in b-space can be expressed by

$$\frac{d^2\sigma_{\rm tot}}{d^2b} = 2\langle t\rangle\,. \tag{3}$$

Finally, the single dissociative cross-section is given by

$$\frac{d^2\sigma_{\rm diff}}{d^2b} = \sum_{P\neq H} |\langle P|\hat{T}|H\rangle|^2\,, \tag{4}$$

where the summation is over all possible particles H in the final states, excluding the initial hadron P, which would correspond to elastic scattering. As a consequence, it is possible to write that[35]

$$\frac{d^2\sigma_{\rm diff}}{d^2b} = \langle t^2\rangle - \langle t\rangle^2\,, \tag{5}$$

i.e. the single dissociation cross-section is given by the variance of the eigenvalues.

In order to estimate the cross-sections in the Good–Walker approach we must assume a model for the factors $|C_k|^2$, which are associated to the probability of finding the eigenstate $|\psi_k\rangle$ in the beam particle state. The description of this probability is directly associated to the modeling of the internal degrees of freedom of the particle. Moreover, we also have to describe the interactions between these degrees of freedom. In what follows, we will consider the model discussed in detail in Ref. 35 (see also Ref. 47). Let us consider that at the instant of interaction, the incident particles can be described by the configurations $\mathbb{C}_1$ and $\mathbb{C}_2$, which are elements of a set of configurations $\{\mathbb{C}_1\}$ and $\{\mathbb{C}_2\}$. Each configuration has a probability associated, $P_h(\mathbb{C}_i)$, in the same sense that $|C_k|^2$ is the probability associated to $|\psi_k\rangle$. With this, we can make the following association in all Good–Walker formulae

$$\sum_j |C_j|^2 \to \int d\mathbb{C}_1 \int d\mathbb{C}_2\, P_{h1}(\mathbb{C}_1) P_{h2}(\mathbb{C}_2)\,, \tag{6}$$

where it is assumed that all possible configurations can be represented by a continuum distribution.

Considering the partonic structure of the interacting hadrons, we expect that the number of elementary interactions will depend on the impact parameter of the collision and on the configurations $\mathbb{C}_1$ and $\mathbb{C}_2$ of the hadrons, which we shall denote by the function $n(s, b, \mathbb{C}_1, \mathbb{C}_2)$. We also expect that the amplitude eigenstates, at leading order, follows $t(s, b, \mathbb{C}_1, \mathbb{C}_2) \approx n(s, b, \mathbb{C}_1, \mathbb{C}_2)$. In order to take into account the multiple interactions between the partons, we will assume that $t(s, b, \mathbb{C}_1, \mathbb{C}_2)$ is given by the eikonal form

$$t(s, b, \mathbb{C}_1, \mathbb{C}_2) = 1 - \exp\left[-\frac{n(s, b, \mathbb{C}_1, \mathbb{C}_2)}{2}\right]. \tag{7}$$

It is also assumed that the energy and impact parameter dependency of the n function can be factorized from the configurations of the particles, $n(s, b, \mathbb{C}_1, \mathbb{C}_2) = \langle n(s, b)\rangle \alpha(\mathbb{C}_1, \mathbb{C}_2)$, where $\langle n(s, b)\rangle$ is the average number of interactions and the

function $\alpha(\mathbb{C}_1, \mathbb{C}_2)$ associates an unique real positive number for each combination of $\mathbb{C}_1$ and $\mathbb{C}_2$. Therefore, $\alpha(\mathbb{C}_1, \mathbb{C}_2)$ works as a mapping from the set of configurations to the set of real positive numbers. This factorization allows us to write the integrals over the particle configurations in terms of an integral over the real number α by defining the probability distribution $p(\alpha)$:

$$p(\alpha) = \int d\mathbb{C}_1 \int d\mathbb{C}_2 P_{h1}(\mathbb{C}_1) P_{h2}(\mathbb{C}_2) \delta[\alpha(\mathbb{C}_1, \mathbb{C}_2) - \alpha] \,, \tag{8}$$

which describes the fluctuations inside the hadrons and that must satisfy

$$\int_0^\infty d\alpha \, p(\alpha) = 1 \,, \quad \int_0^\infty d\alpha \, \alpha p(\alpha) = 1 \,. \tag{9}$$

These constraints follow from the normalization of $P_h(\mathbb{C})$,

$$\int d\mathbb{C} \, P_h(\mathbb{C}) = 1 \,, \tag{10}$$

and from the definitions of average value of the number of elementary interactions,

$$\int d\mathbb{C}_1 \int d\mathbb{C}_2 \, P_{h1}(\mathbb{C}_1) P_{h2}(\mathbb{C}_2) n(s, b, \mathbb{C}_1, \mathbb{C}_2) = \langle n(s, b) \rangle \,. \tag{11}$$

The form of the probability distribution $p(\alpha)$ is still an open problem. However, this distribution must be defined for positive values of its variable (α) and we expect that it has the appropriate limit, $p(\alpha) \to \delta(\alpha - 1)$, when its variance goes to zero, which corresponds to the case of no-fluctuations. It is also interesting to have an analytical structure that allows us, in some extent, to obtain analytical (closed) expressions. As in Ref. 35, we will assume that $p(\alpha)$ can be described by a gamma distribution, with variance w,

$$p(\alpha) = \frac{1}{w\Gamma(1/w)} \left(\frac{\alpha}{w} \right)^{-1+1/w} e^{-\alpha/w} \,, \tag{12}$$

which has the aforementioned properties. Moreoever, it is straightforward to show that Eq. (12) satisfies the constraints of Eq. (9) and that for $w \to 0$ it shows the expected limit, corresponding to the case of no fluctuations which implies no dissociative process. Using Eq. (12) we obtain that the average values $\langle t \rangle$ and $\langle t^2 \rangle$ are given by

$$\langle t \rangle = 1 - \left(1 + \frac{\langle n(s, b) \rangle w}{2} \right)^{-1/w} , \tag{13}$$

$$\langle t^2 \rangle = (1 + \langle n(s, b) \rangle w)^{-1/w} - \left(1 + \frac{\langle n(s, b) \rangle w}{2} \right)^{-2/w} . \tag{14}$$

In order to estimate the cross-sections we must consider a model to the average number of elementary interactions $\langle n(s, b) \rangle$. The treatment of this quantity is still an open problem in the literature. As in Ref. 35, we will assume the *ansatz* that the average number of interactions can be factorized in two parts: the overlap function

that depends on b only and describes how the partons are distributed inside the hadron in the b-plane and the eikonal cross-section (a function of energy only) that describes the interaction between the interacting hadrons at a given CM energy $\sqrt{s}$. Therefore, we will assume that

$$\langle n(s,b)\rangle = \sigma_{\rm eik}(s)\frac{b^3}{96\pi r_0^5}K_3\left(\frac{b}{r_0}\right), \tag{15}$$

with the eikonal cross-section containing information from both the perturbative and nonperturbative regimes of QCD. In our study, we will assume that this quantity can be expressed as a combination of hard and soft contributions

$$\sigma_{\rm eik}(s) = \sigma_{\rm pQCD}(s) + \sigma_{\rm soft}(s)\,, \tag{16}$$

where $\sigma_{\rm pQCD}$ accounts for the mid and high-energy behavior of the elastic scattering amplitude, whilst the $\sigma_{\rm soft}$ is expected to be meaningful only at low energies. For the soft contribution, we will assume that it can be written by means of a parametrization based on Regge–Gribov phenomenology. Thus we take

$$\sigma_{\rm soft}(s) = A_1\left(\frac{s}{s_0}\right)^{-\delta_1} \pm A_2\left(\frac{s}{s_0}\right)^{-\delta_2} + \sigma_0\,, \tag{17}$$

where the plus and minus signs correspond to $\bar{p}p$ and pp scatterings, respectively. Furthermore, in the present analysis A_1, A_2, δ_1, δ_2 and σ_0 are fitting parameters and we assume $s_0 = 25$ GeV^2. The first and second terms correspond to even and odd-under-crossing Reggeon exchange, respectively, and σ_0 is associated with the critical Pomeron exchange. Bearing in mind that these Reggeons do not appear directly in the Born-level amplitudes, they must be seen as effective contributions. On the other hand, for the hard sector, which is responsible for the high-energy dynamics, we will assume that it can be expressed by means of the minijet cross-section obtained using perturbative QCD. More specifically, it is obtained through the convolution of the elementary cross-section for the QCD subprocesses, respectively with their partonic distributions as follows:

$$\begin{aligned}\sigma_{\rm pQCD}(s) &= \sigma_{\rm minijet}(s)\\ &= \sum_{i,j=q,\bar{q},g}\frac{1}{1+\delta_{ij}}\int_0^1 dx_1\int_0^1 dx_2\int_{Q^2_{\rm min}}^{\infty} d|\hat{t}|\frac{d\hat{\sigma}_{ij}}{d|\hat{t}|}(\hat{s},\hat{t})\\ &\quad\times f_{i/P}(x_1,|\hat{t}|)f_{j/T}(x_2,|\hat{t}|)\Theta\left(\frac{\hat{s}}{2}-|\hat{t}|\right),\end{aligned} \tag{18}$$

where x_1 and x_2 are the momentum fractions of the partons inside of hadrons P and T, $\hat{s}$ and $\hat{t}$ are the Mandelstam variables for the partonic collision, $d\hat{\sigma}_{ij}/d|\hat{t}|$ is the differential cross-section for ij scattering, and $f_{i/h}$ stands for the PDFs of the hadron h. The integration over $|\hat{t}|$ satisfy the physical condition $\hat{s} > 2|\hat{t}| > 2Q^2_{\rm min}$, where $\hat{s} = x_1x_2s$ and $Q^2_{\rm min}$ is the minimal momentum transfer in the hard scattering, here assumed to be 1.69 GeV^2. As a consequence, one has that $(x_1x_2)_{\rm min} = 2Q^2_{\rm min}/s$,

which implies that the minimum values of x_i can be of the order of 10^{-8} at the LHC typical energy domain, which is the x-range for the PDFs presented in Fig. 1. It is important to emphasize that we have verified that our predictions are not very sensitive to the choice of the momentum-cutoff $Q_{\rm min}$ in the interval $1.0 \leq Q_{\rm min} \lesssim 1.5$ GeV, in agreement with the results presented in Ref. 32. Since the gluon distribution becomes dominant in the $x \to 0$ asymptotic regime, we will include in our calculations all process with at least one gluon in the initial state, i.e. we select the processes $gg \to gg$ (gluon–gluon fusion), $qg \to qg$ and $\bar{q}g \to \bar{q}g$ (quark–gluon scattering) and for completeness $gg \to \bar{q}q$ (gluon fusion into a quark pair).[32–34] However, these subprocesses at low transferred momenta are plagued by infrared divergences and must be properly regularized. To tame these divergences we follow the dynamical gluon mass approach proposed by Luna *et al.*[30–34] We have verified that our results are not dependent on the treatment of these divergences due to the bound $|\hat{t}| \geq Q^2_{\rm min}$. One has that the uncertainties related to the value of $Q_{\rm min}$ and to the treatment of the infrared regime are smaller than those associated to the choice of the PDFs.

The main input in the calculations of the hard contribution for the eikonal cross-section is the description of the partonic structure modeled by the parton distribution functions. As emphasized in the Introduction, our goal is to analyze the impact of different parametrizations on the hadronic cross-sections. Presently, there are many available PDFs sets, but in our study we shall investigate the effects of three leading-order post-LHC fine-tuned parametrizations, namely CT14,[44] NNPDF31[45] and MMHT.[46]

3. Results

In order to determine the parameters of the model, w, A_1, A_2, δ_1, δ_2 and σ_0 we consider fits to experimental data for the pp and $\bar{p}p$ total cross-sections. The dataset comprise data on $\sigma_{\rm tot}$ obtained only in accelerator experiments covering the energy range from 5 GeV to 13 TeV. Data below 1.8 TeV were obtained from the Particle Data Group,[36] while for the LHC energies, we included data obtained by TOTEM Collaboration in the energies of 2.76, 7, 8 and 13 TeV (Refs. 1, 2, 37–40) and data by ATLAS Collaboration at 7 and 8 TeV (Refs. 41 and 42). Statistical and systematical uncertainties were added in quadrature. The model has six free parameters, being five of them associated to the description of the soft cross-section. All fits were performed using the class TMinuit from ROOT Framework through the MIGRAD algorithm. We consider a χ^2 fitting procedure where the data reduction assumes an interval $\chi^2 - \chi^2_{\rm min} = 7.04$ corresponding, in the case of normal errors, to the projection of the χ^2 hypersurface containing 68.3% of probability, namely uncertainties in the free parameters with 1σ of confidence level.

The parameters determined in fits to $\sigma_{\rm tot}$ data are displayed in Table 1. In Fig. 2 we show the comparison of experimental data with the fit results for the three PDF sets considered. Considering the central curves in each case, we see that CT14 and

Table 1. Best fit parameters to $\sigma_{\rm tot}$ from pp and $\bar{p}p$ scatterings with PDFs NNPDF31,[45] CT14[44] and MMHT.[46] The quality fit estimator chi-squared per degree-of-freedom, χ^2/ν, are also included where $\nu = 171$ stands for the number of degrees of freedom.

PDF	NNPDF31	CT14	MMHT
w	1.42 ± 0.10	1.83 ± 0.10	1.43 ± 0.10
A_1 [mb]	27.7 ± 2.2	29.8 ± 2.7	25.4 ± 2.4
δ_1	1.25 ± 0.10	1.45 ± 0.11	1.61 ± 0.13
A_2 [mb]	22.8 ± 1.6	26.0 ± 1.8	22.8 ± 1.5
δ_2	0.580 ± 0.045	0.582 ± 0.044	0.576 ± 0.043
σ_0 [mb]	83.4 ± 2.0	91.7 ± 2.2	85.3 ± 2.0
χ^2/ν	3.80	3.75	6.02

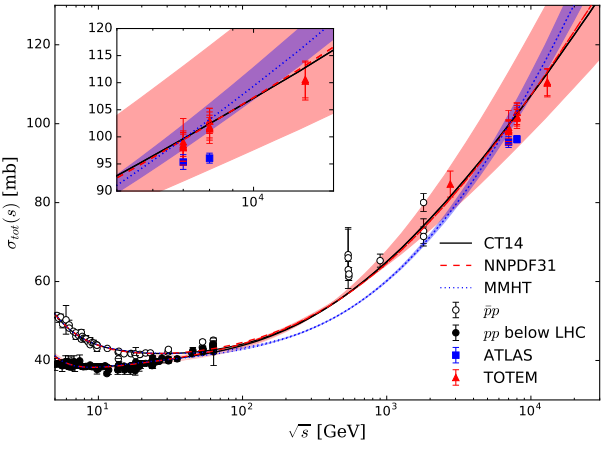

Fig. 2. Result of fit to $\sigma_{\rm tot}$ data from pp and $\bar{p}p$ scattering considering different parametrizations for the partonic structure of the proton.

NNPDF31 give similar descriptions to $\sigma_{\rm tot}$ in the entire energy range considered. On the other hand, the MMHT result presents a different increase rate with energy and it crosses the CT14 and NNPDF31 results at approximately 7 TeV. The differences become evident at energies higher than 100 GeV. The associated eikonal cross-section is presented in the left panel of Fig. 3 and the soft and hard components in the right panel of the same figure. As expected, the soft contribution dominates at low energies and becomes constant (σ_0) as the energy increases. Moreover, by the energy of $\sqrt{s} \sim 1$ TeV, the hard (pQCD) component is already dominant in the eikonal cross-section.

Our predictions to $\sigma_{\rm el}$ and $\sigma_{\rm diff}$ are presented, respectively, on the left and right panel of Fig. 4. For the central curves and LHC energies, the MMHT set shows the largest magnitude of $\sigma_{\rm el}$ compared with the others and CT14 the lowest. Similar

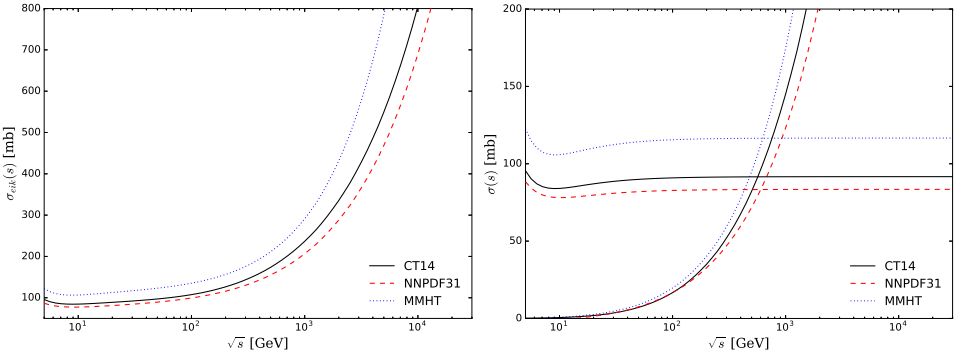

Fig. 3. Left panel: Energy dependence of the eikonal cross-section for pp collisions. Right panel: Hard and soft contributions for the total pp cross-section.

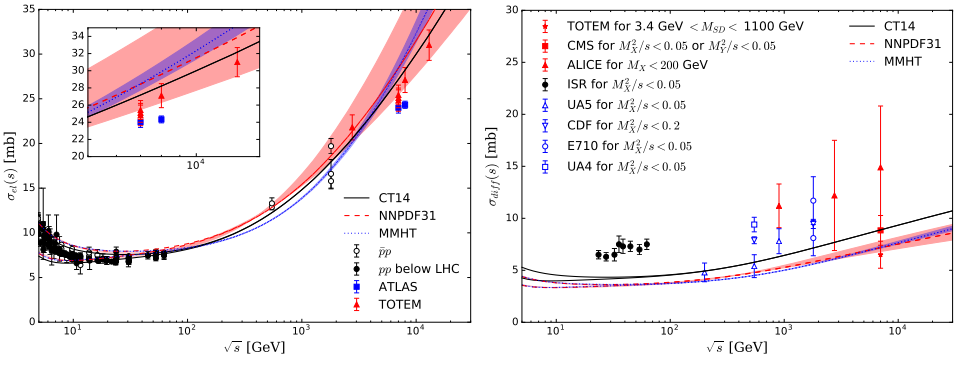

Fig. 4. Predictions for the elastic (left panel) and diffractive dissociation (right panel) cross-sections. Data for $\sigma_{\rm el}$ from Refs. 2, 36–39 and $\sigma_{\rm diff}$ from Refs. 48–57.

to the total cross-section, $\sigma_{\rm el}$ from CT14 and NNPDF31 present similar increase rate but now they differ in the magnitude. The TOTEM data for $\sigma_{\rm el}$ are better described by the result obtained with CT14. In respect to $\sigma_{\rm diff}$, the prediction with CT14 presents larger magnitude when compared to the other cases, with NNPDF31 and MMHT predictions being similar.

The predictions for impact parameter dependence of the elastic and single diffractive cross-sections for $\sqrt{s} = 13$ TeV are presented in Fig. 5. As already verified in Ref. 35, the elastic cross-section is mainly central, while the single diffractive cross-section is more peripheral. The magnitude of the maximum is dependent on the PDF considered, but its position occurs for a similar value of b in the LHC energy. However, such conclusion is not valid for other energies. As shown in Fig. 6, where we present the energy dependence of the single diffractive cross-section, from Tevatron to cosmic rays energies, the position of the maximum changes with energy and is dependent on the modeling of the partonic structure, with the magnitude of the SD cross-section at $b = 0$ decreasing at larger energies. Such distinct behaviors

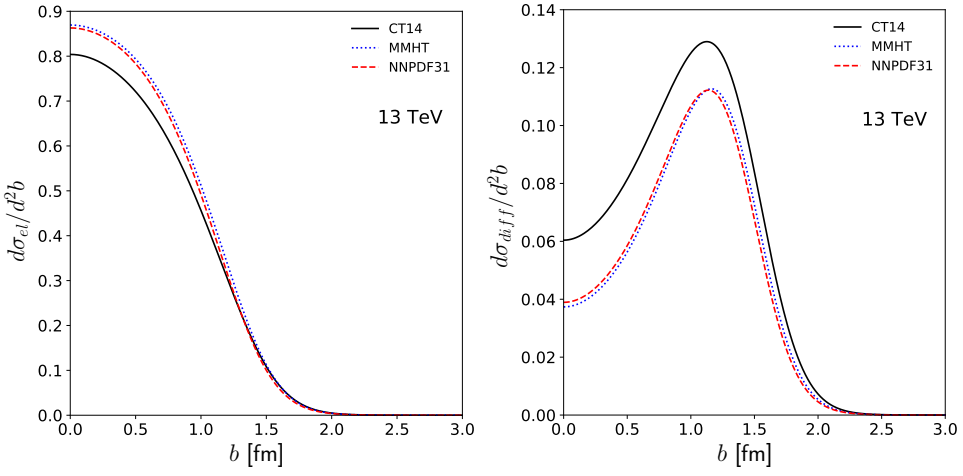

Fig. 5. Predictions for impact parameter dependence of the elastic (left panel) and single diffractive (right panel) cross-sections for the three distinct PDFs and $\sqrt{s} = 13$ TeV.

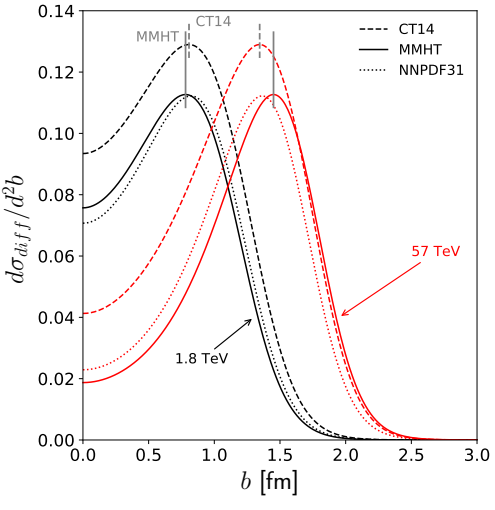

Fig. 6. Energy evolution of the maximum of $d\sigma_{\rm diff}/d^2b$ for three PDFs. The vertical lines correspond to the value of b where the distribution is maximum. The maximum for NNPDF31, not shown, is close to the value of MMHT at 1.8 TeV and close to the value of CT14 at 57 TeV.

are directly associated to the x-dependence of the PDFs, which is very different at smaller values of x, which are probed at larger energies.

4. Summary

The observed increase of hadronic cross-sections represents one of the main current trend of interests in both theoretical and experimental Particle Physics. Nonetheless, models based on QCD represent a possible approach to properly study the

high-energy regime of hadronic scatterings. In this work we have complemented the analysis performed in Ref. 35, where we have proposed a model based on the Good–Walker approach to describe the hadronic cross-sections, by investigating the impact of distinct models for the partonic structure of the proton on the asymptotic behavior of the total, elastic and single diffractive cross-sections. Bearing in mind that the bulk of $\sigma_{\rm tot}$ data presently consists one of the best and most complete datasets covering the high-energy range of pp and $\bar{p}p$ scatterings, we carried out fits to $\sigma_{\rm tot}^{pp,\bar{p}p}$ paying attention to the different behaviors implied by distinct partonic distribution inside hadrons, namely CT14, NNPDF31 and MMHT. The best-fitted parameter to $\sigma_{\rm tot}$ were also used to derive free parameter predictions for the total elastic and diffractive cross-sections. Our results demonstrated that the description of the hadronic cross-sections is sensitive to the description of the partonic structure of the hadrons, in particular, to the small-x behavior of the PDFs, which is directly related to the description of the QCD dynamics at high energies.

Acknowledgments

This research was partially supported by the Conselho Nacional de Desenvolvimento Científico e Tecnológico (CNPq), Fundação de Amparo — Pesquisa do Estado do Rio Grande do Sul (FAPERGS) and Instituto Nacional de Ciência e Tecnologia — Física Nuclear e Aplicações (INCT-FNA) (process Nos. 464898/2014-5 and 155628/2018-6).

References

1. TOTEM Collab. (G. Antchev *et al.*), *Eur. Phys. J. C* **79**, 785 (2019).
2. TOTEM Collab. (G. Antchev *et al.*), *Eur. Phys. J. C* **79**, 103 (2019).
3. TOTEM Collab. (G. Antchev *et al.*), *Eur. Phys. J. C* **79**, 861 (2019).
4. TOTEM Collab. (G. Antchev *et al.*), *Eur. Phys. J. C* **80**, 91 (2020).
5. H. Cheng and T. T. Wu, *Phys. Rev. Lett.* **24**, 1456 (1970).
6. C. Bourrely, J. Soffer and T. T. Wu, *Phys. Rev. Lett.* **54**, 757 (1985).
7. A. Donnachie and P. V. Landshoff, *Z. Phys. C* **2**, 55 (1979) [Erratum: *ibid.* **2**, 372 (1979)].
8. A. Donnachie and P. V. Landshoff, *Phys. Lett. B* **296**, 227 (1992).
9. A. Donnachie and P. V. Landshoff, *Phys. Lett. B* **727**, 500 (2013) [Erratum: *ibid.* **750**, 669 (2015)].
10. J. R. Cudell, V. Ezhela, P. Gauron, K. Kang, Yu. V. Kuyanov, S. Lugovsky, B. Nicolescu and N. Tkachenko, *Phys. Rev. D* **65**, 074024 (2002).
11. M. M. Block and F. Halzen, *Phys. Rev. D* **86**, 014006 (2012).
12. M. M. Block and F. Halzen, *Phys. Rev. D* **86**, 051504 (2012).
13. R. F. Avila, E. G. S. Luna and M. J. Menon, *Phys. Rev. D* **67**, 054020 (2003).
14. E. G. S. Luna and M. J. Menon, *Phys. Lett. B* **565**, 123 (2003).
15. D. A. Fagundes, M. J. Menon and P. V. R. G. Silva, *Nucl. Phys. A* **966**, 185 (2017).
16. D. A. Fagundes, M. J. Menon and P. V. R. G. Silva, *Int. J. Mod. Phys. A* **32**, 1750184 (2017).
17. M. Broilo, E. G. S. Luna and M. J. Menon, *Phys. Lett. B* **781**, 616 (2018).
18. M. Broilo, E. G. S. Luna and M. J. Menon, *Phys. Rev. D* **98**, 074006 (2018).

19. R. Fiore, L. L. Jenkovszky, R. Orava, E. Predazzi, A. Prokudin and O. Selyugin, *Int. J. Mod. Phys. A* **24**, 2551 (2009).
20. E. G. S. Luna, V. A. Khoze, A. D. Martin and M. G. Ryskin, *Eur. Phys. J. C* **59**, 1 (2009).
21. E. Gotsman, E. M. Levin and U. Maor, *Phys. Rev. D* **49**, R4321 (1994).
22. P. L'Heureux, B. Margolis and P. Valin, *Phys. Rev. D* **32**, 1681 (1985).
23. B. Margolis, P. Valin, M. M. Block, F. Halzen and R. S. Fletcher, *Phys. Lett. B* **213**, 221 (1988).
24. M. M. Block, E. M. Gregores, F. Halzen and G. Pancheri, *Phys. Rev. D* **60**, 054024 (1999).
25. L. Durand and H. Pi, *Phys. Rev. D* **38**, 78 (1988).
26. L. Durand and H. Pi, *Phys. Rev. D* **40**, 1436 (1989).
27. A. Corsetti, A. Grau, G. Pancheri and Y. N. Srivastava, *Phys. Lett. B* **382**, 282 (1996).
28. D. A. Fagundes, A. Grau, S. Pacetti, G. Pancheri and Y. N. Srivastava, *Phys. Rev. D* **88**, 094019 (2013).
29. D. A. Fagundes, A. Grau, G. Pancheri, Y. N. Srivastava and O. Shekhovtsova, *Phys. Rev. D* **91**, 114011 (2015).
30. E. G. S. Luna, A. F. Martini, M. J. Menon, A. Mihara and A. A. Natale, *Phys. Rev. D* **72**, 034019 (2005).
31. E. G. S. Luna, A. L. dos Santos and A. A. Natale, *Phys. Lett. B* **698**, 52 (2011).
32. C. A. S. Bahia, M. Broilo and E. G. S. Luna, *Phys. Rev. D* **92**, 074039 (2015).
33. M. Broilo, D. A. Fagundes, E. G. S. Luna and M. J. Menon, *Eur. Phys. J. C* **79**, 1033 (2019).
34. M. Broilo, D. A. Fagundes, E. G. S. Luna and M. J. Menon, *Phys. Lett. B* **799**, 135047 (2019).
35. M. Broilo, V. P. Goncalves and P. V. R. G. Silva, *Phys. Rev. D* **101**, 074034 (2020).
36. Particle Data Group (M. Tanabashi *et al.*), *Phys. Rev. D* **98**, 030001 (2018).
37. TOTEM Collab. (G. Antchev *et al.*), *Europhys. Lett.* **101**, 21004 (2013).
38. TOTEM Collab. (G. Antchev *et al.*), *Phys. Rev. Lett.* **111**, 012001 (2013).
39. TOTEM Collab. (G. Antchev *et al.*), *Nucl. Phys. B* **899**, 527 (2015).
40. TOTEM Collab. (G. Antchev *et al.*), *Eur. Phys. J. C* **76**, 661 (2016).
41. ATLAS Collab. (G. Aad *et al.*), *Nucl. Phys. B* **889**, 486 (2014).
42. ATLAS Collab. (M. Aaboud *et al.*), *Phys. Lett. B* **761**, 158 (2016).
43. M. L. Good and W. D. Walker, *Phys. Rev.* **120**, 1857 (1960).
44. S. Dulat, T.-J. Hou, J. Gao, M. Guzzi, J. Huston, P. Nadolsky, J. Pumplin, C. Schmidt, D. Stump and C. P. Yuan, *Phys. Rev. D* **93**, 033006 (2016).
45. R. D. Ball *et al.*, *Eur. Phys. J. C* **77**, 663 (2017), arXiv:1706.00428 [hep-ph].
46. L. A. Harland-Lang, A. D. Martin, P. Motylinski and R. S. Thorne, *Eur. Phys. J. C* **75**, 204 (2015).
47. P. Lipari and M. Lusignoli, *Phys. Rev. D* **80**, 074014 (2009).
48. J. C. M. Armitage *et al.*, *Nucl. Phys. B* **194**, 365 (1982).
49. N. Cartiglia, arXiv:1305.6131.
50. ALICE Collab. (B. Abelev *et al.*), *Eur. Phys. J. C* **73**, 2456 (2013).
51. CMS Collab. (V. Khachatryan *et al.*), *Phys. Rev. D* **92**, 012003 (2015).
52. UA5 Collab. (R. E. Ansorge *et al.*), *Z. Phys. C* **33**, 175 (1986).
53. UA5 Collab. (G. J. Alner *et al.*), *Phys. Rep.* **154**, 247 (1987).
54. UA4 Collab. (D. Bernard *et al.*), *Phys. Lett. B* **186**, 227 (1987).
55. E-710 Collab. (N. A. Amos *et al.*), *Phys. Lett. B* **243**, 158 (1990).
56. E710 Collab. (N. A. Amos *et al.*), *Phys. Lett. B* **301**, 313 (1993).
57. CDF Collab. (F. Abe *et al.*), *Phys. Rev. D* **50**, 5535 (1994).